Microtubule plus-end tracking of end-binding protein 1 (EB1) is regulated by CDK5 regulatory subunit-associated protein 2

Received for publication, September 21, 2016, and in revised form, March 15, 2017 Published, Papers in Press, March 20, 2017, DOI 10.1074/jbc.M116.759746

Ka-Wing Fong[1], **Franco K. C. Au, Yue Jia, Shaozhong Yang, Liying Zhou, and Robert Z. Qi**[2]

From the Division of Life Science and State Key Laboratory of Molecular Neuroscience, The Hong Kong University of Science and Technology, Clear Water Bay, Kowloon, Hong Kong, China

Edited by Velia M. Fowler

Microtubules are polar cytoskeleton filaments that extend via growth at their plus ends. Microtubule plus-end-tracking proteins (+TIPs) accumulate at these growing plus ends to control microtubule dynamics and attachment. The +TIP end-binding protein 1 (EB1) and its homologs possess an autonomous plus-end-tracking mechanism and interact with other known +TIPs, which then recruit those +TIPs to the growing plus ends. A major +TIP class contains the S*X*IP (Ser-*X*-Ile-Pro, with *X* denoting any amino acid residue) motif, known to interact with EB1 and its homologs for plus-end tracking, but the role of S*X*IP in regulating EB1 activities is unclear. We show here that an interaction of EB1 with the S*X*IP-containing +TIP CDK5 regulatory subunit-associated protein 2 (CDK5RAP2) regulates several EB1 activities, including microtubule plus-end tracking, dynamics at microtubule plus ends, microtubule and α/β-tubulin binding, and microtubule polymerization. The S*X*IP motif fused with a dimerization domain from CDK5RAP2 significantly enhanced EB1 plus-end-tracking and microtubule-polymerizing and bundling activities, but the S*X*IP motif alone failed to do so. An S*X*IP-binding-deficient EB1 mutant displayed significantly lower microtubule plus-end tracking than the wild-type protein in transfected cells. These results suggest that EB1 cooperates with CDK5RAP2 and perhaps other S*X*IP-containing +TIPs in tracking growing microtubule tips. We also generated plus-end-tracking chimeras of CDK5RAP2 and the adenomatous polyposis coli protein (APC) and found that overexpression of the dimerization domains interfered with microtubule plus-end tracking of their respective S*X*IP-containing chimeras. Our results suggest that disruption of S*X*IP dimerization enables detailed investigations of microtubule plus-end-associated functions of individual S*X*IP-containing +TIPs.

Microtubules are polar filaments with the plus end located distally from microtubule organizing centers and often growing toward the cell periphery. A diverse group of proteins accumulate at the growing plus ends and thus are known as microtubule plus-end-tracking proteins (+TIPs)[3] (1, 2). Positioned to control microtubule dynamics and attachment to various subcellular structures, +TIPs play important roles in a multitude of cellular activities, including intracellular transport, cell division, polarity establishment, cell motility, and morphogenesis. Among +TIPs, end-binding proteins (EBs) such as EB1 are highly conserved proteins that recognize and accumulate at growing microtubule tips through an autonomous mechanism (3). Moreover, EBs are master integrators of plus-end-tracking complexes, and a variety of other +TIPs are recruited to the plus ends by interacting with EBs. A large group of +TIPs contains the S*X*IP (Ser-*X*-Ile-Pro, *X* denotes any amino acid residue) motif encompassed in basic and Ser-rich sequences for binding to EBs (4–6). Examples of S*X*IP-containing +TIPs are CDK5RAP2 (also known as Cep215), the adenomatous polyposis coli (APC) tumor suppressor protein, MACF (known as ACF7 in mouse), and CLIP-associating proteins CLASP1/2 (1, 5, 7).

Being a prototypic +TIP, EB1 localizes at all growing microtubule plus ends and interacts with virtually all other +TIPs (1, 2, 8). The structure of EB1 comprises a calponin-homology domain responsible for microtubule binding, a coiled-coil region, which mediates its homodimerization, and a unique EB homology (EBH) domain for binding to other +TIPs (4, 6, 9–12). In the S*X*IP-EB1 complexes, the Ile/Leu-Pro dipeptide of the S*X*IP motif is inserted into the hydrophobic pocket formed by the EBH domain, and Ser of the motif forms a network of hydrogen bonds with several conserved residues of the EBH domain (4, 6, 12).

EB1 possesses an intrinsic activity of promoting microtubule assembly (11, 13). Hence, at the plus ends, EB1 enhances microtubule growth and prevents microtubules from pausing (14–17). The microtubule-polymerizing activity of EB1 is controlled by an autoinhibitory mechanism imparted by its tail region, and the autoinhibition can be relieved by binding of the tail to other +TIPs, such as p150Glued or APC (6, 11, 12, 18). This suggests the regulation of EB1 by its +TIP binding partners.

CDK5RAP2 displays both centrosomal localization and microtubule plus-end tracking. It is a pericentriolar-material

This work was supported by grants from the Research Grants Council (General Research Fund and Theme-based Research Scheme) of Hong Kong, the National Key Basic Research Program of China (2013CB530900), the University Grants Committee (Area of Excellence Scheme) of Hong Kong, the Innovation and Technology Commission (ITCPD/17–9) of Hong Kong, and the TUYF Charitable Trust. The authors declare that they have no conflicts of interest with contents of this article.

This article contains supplemental Movies 1–10.

[1] Present address: Division of Hematology/Oncology, Dept. of Medicine, Northwestern University Feinberg School of Medicine, Chicago, IL 60611.

[2] To whom correspondence should be addressed. Tel.: 852-2358-7273; Fax: 852-2358-1552; E-mail: qirz@ust.hk.

[3] The abbreviations used are: +TIPs, microtubule plus-end-tracking proteins; APC, adenomatous polyposis coli protein; CAP-Gly, cytoskeleton-associated protein glycine-rich; CDK5RAP2, CDK5 regulatory subunit-associated protein 2; EB1, end-binding protein 1; EBH, EB homology; FRAP, fluorescence recovery after photobleaching.

component that interacts with γ-tubulin ring complexes to regulate microtubule nucleation (19, 20), and it contains the S*X*IP motif for EB1 binding to track-growing microtubule plus ends and regulated microtubule dynamics (7). In this report we further analyze the plus-end-tracking mechanism of CDK5RAP2 and demonstrate that a dimerization domain is required in addition to the S*X*IP motif to form a highly active plus-end-tracking module. Remarkably, the plus-end-tracking activity of EB1 is differentially regulated by the monomeric and dimeric/multimeric forms of its bound S*X*IP motif. We also show that disruption of the dimerization/multimerization serves as a specific approach to interfere with the plus-end tracking of individual S*X*IP-containing +TIPs, such as CDK5RAP2, without affecting the plus-end tracking of other S*X*IP-containing +TIPs.

Results

Dissecting the plus-end-tracking module of CDK5RAP2

The CDK5RAP2 fragment 926–1208 (referred to hereafter as M1) contains the S*X*IP motif spanning the region of 926–956 and binds to EB1 (7). Time-lapse microscopy showed a robust microtubule plus-end tracking of M1 (supplemental Movie S1), in agreement with its staining to the distal tips of microtubules (7). To further dissect this plus-end-tracking module, we generated two truncation constructs, 926–1015 and 956–1208, and designated them as M2 and M3, respectively (Fig. 1*A*). Of them, M2 contains the S*X*IP motif, and it showed similar EB1-binding activities as M1 in a co-immunoprecipitation assay (Fig. 1*A*). In contrast, M3, which lacks the S*X*IP motif, failed to bind to EB1 (Fig. 1*A*). Therefore, M2 is sufficient for EB1 association. We proceeded to examine the microtubule tip-tracking activities by immunofluorescence and time-lapse imaging, and cells transfected with the CDK5RAP2 fragments at low levels were analyzed. M1 exhibited a robust activity of tracking microtubule plus ends (Fig. 1*A* and supplemental Movie S1). M2 tracked the plus ends, albeit very weakly and with a substantially lower activity than M1 (~83% lower than M1; Fig. 1*B* and supplemental Movie S2). In agreement with the lack of EB1-binding activities, M3 did not exhibit any tip-tracking activity (Fig. 1*B* and supplemental Movie S3).

The above observations revealed that the carboxyl-terminal truncation in M1 significantly reduces its plus-end-tracking activity, although the truncation does not affect its EB1-binding activity. We set out to investigate the role of the truncated region in microtubule plus-end-tracking function. Immunoprecipitation of ectopically expressed M1 is able to co-immunoprecipitate endogenous CDK5RAP2. This observation prompted us to investigate whether M1 contains a dimerization domain. To test this, we co-expressed two M1 constructs, one tagged with FLAG and the other with GFP. Immunoprecipitation of FLAG-M1 through the ectopic tag showed the co-precipitation of GFP-M1 (Fig. 1*C*). When GFP-M1 was cotransfected with M2 and M3, GFP-M1 was found in the anti-FLAG immunoprecipitate of M3 but not in that of M2 (Fig. 1*C*). Direct interaction was then tested using purified recombinant proteins. In the assay, GST-M1 interacted with His_6-M1 and His_6-M3 but not with His_6-M2 (Fig. 1*D*), consistent with the co-immunoprecipitation results. As a control, GST did not bind to any of these CDK5RAP2 fragments (Fig. 1*D*). These results demonstrated that M1 forms a homodimer or homomultimers through the M3 region.

Effect of M1 and its fragments on the plus-end tracking of EB1

Because M1 and M2 exhibited dramatically different plus-end-tracking activities, we explored their potential impacts on the plus-end-tracking behavior of EB1. In transfected cells, M1 displayed an almost identical pattern as EB1 (Fig. 2*A*). Furthermore, expression of M1 led to a remarkable increase of EB1 signals at the plus ends; the signal intensity and the comet tail length of EB1 were increased by ~96 and ~91%, respectively (Fig. 2*A*). In contrast, when M2 was expressed the comet-tail signals of EB1 were significantly hampered (~74% reduction of the signal intensity; Fig. 2*A*). Similar effects were observed when the CDK5RAP2 fragments were expressed in cells in which the expression of endogenous CDK5RAP2 was suppressed by RNAi (Fig. 2*A*). When the EB1-binding-deficient mutants of M1 and M2 (*i.e.* L938A/P939A) were tested, they did not show these effects (data not shown). Therefore, these S*X*IP-containing constructs can make notable impacts on the plus-end tracking of their bound EB1. Any significant change in plus-end-associated EB1 signals was not observed by M3 expression (Fig. 2*A*).

The plus-end association of EB1 and its homologs is highly dynamic, and the dynamic behaviors depend at least on EB diffusion and interaction with other proteins (21, 22). To evaluate the plus-end dynamics of EB1 in complex with CDK5RAP2 fragments, we performed fluorescence recovery after photobleaching (FRAP) analyses. Photobleaching was done at the peripheral regions of U2OS cells that stably expressed EB1-GFP at a low level (7) and were transiently transfected with mCherry constructs as indicated. Whereas the expression of mCherry-M1 reduced the rate of EB1-GFP fluorescence recovery at the microtubule distal tips, the expression of mCherry-M2 increased the recovery rate (Fig. 2*B* and supplemental Movie S4). These results revealed the opposite effects of M1 and M2 on EB1 turnover at microtubule plus ends.

To verify the impact of S*X*IP interaction, we created an EB1 mutant deficient of S*X*IP-binding activities by substituting Lys-220 and Arg-222, the conserved residues involved in interaction with the S*X*IP motif (6, 12, 23). Notably, the K220A and R222A mutations do not affect the homodimerization of EB1 (6). The double mutation K220A/R222A abolished the interaction of EB1 with M1 (Fig. 3*A*). This mutational effect on S*X*IP interaction was verified by a binding test using the S*X*IP sequence from APC, and this APC sequence is 2780–2843 and designated as APC(C) (Fig. 3*A*).

Subsequently, we measured the plus-end-tracking activity of EB1 and its K220A/R222A mutant. To avoid dimerization of the expressed EB1 proteins with endogenous EB1 and EB3 (6, 24), the expression of both endogenous proteins was silenced by RNAi. Although the mutant could track growing microtubule plus ends, it displayed a significantly lower tracking activity than the wild-type protein; both the signal intensity and the number of EB1 comets were reduced significantly by the mutation (reduction of the comet intensity by ~74%; Fig. 3*B* and

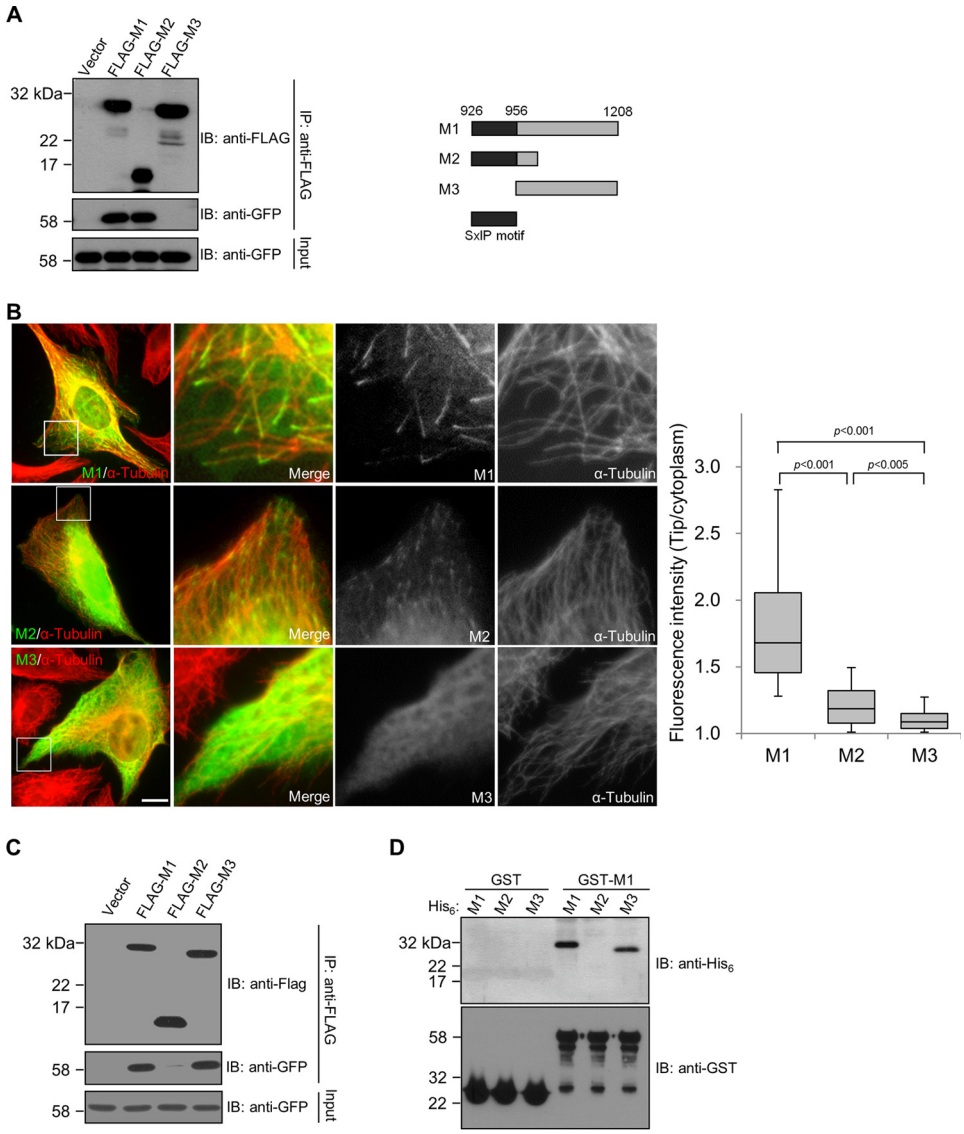

Figure 1. The plus-end-tracking domain of CDK5RAP2 contains an SXIP motif and a dimerization domain. *A*, EB1 binding of CDK5RAP2 fragments were tested by co-immunoprecipitation (*IP*) from the extracts of HEK293T cells co-expressing the CDK5RAP2 fragments (FLAG tagged) and EB1-GFP. The anti-FLAG immunoprecipitates (30%) and the cell extract inputs (5%) were analyzed by immunoblotting (*IB*). Shown on the *right* is a scheme of the CDK5RAP2 fragments. *B*, GFP-tagged M1, M2, and M3 were transiently expressed in U2OS cells. We analyzed cells expressing the proteins at similar levels and measured the fluorescence intensities at the microtubule distal tips and in the cytoplasm. *Boxed areas* are enlarged. *Bar*, 10 μm. The tip/cytoplasm intensity ratios of 50 microtubule tips selected from 5 transfected cells are presented as *box-and-whisker plots*: *boxes* represent the 25th and 75th percentiles, a *line within the boxes* depicts the median, and *whiskers* represent the 10th and 90th percentiles. *p* values were calculated by the Student's unpaired two tails *t* test. *C*, GFP-M1 was cotransfected with FLAG-tagged M1, M2, or M3 into HEK293T cells. After anti-FLAG immunoprecipitation (*IP*), the immunoprecipitates (30%) and the cell extract inputs (5%) were analyzed on immunoblots (*IB*). GFP-M1 was co-immunoprecipitated with FLAG-tagged M1 and M3, but not with FLAG-M2. *D*, an *in vitro* binding assay was conducted with 0.5 μM, each of the purified recombinant proteins His_6-M1, His_6-M2, His_6-M3, GST, and GST-M1. After incubation of the His_6-tagged proteins with the GST proteins as indicated, the GST proteins were pulled down, and the bound proteins were analyzed on anti-His_6 and anti-GST immunoblots (*IB*). His_6-tagged M1 and M3 were specifically found in the GST-M1 pulldowns, whereas His_6-M2 was not detected.

supplemental Movie S5). We also performed the FRAP analysis and found that the fluorescence of the K220A/R222A mutant recovered faster than the wild-type EB1 protein at the plus ends (Fig. 3*C* and supplemental Movie S6). In the absence of S*X*IP interaction, EB1 turns over more rapidly at microtubule plus ends and shows a lower plus-end-tracking activity. It should be noted that these EB1 constructs contain GFP at the protein carboxyl terminus, disrupting the carboxyl-terminal EEY/F-COO^- motif and, thus, excluding the binding of the cytoskeleton-associated protein glycine-rich (CAP-Gly) domain (25, 26).

EB1-SXIP activities toward microtubules

Because M1, M2, and M3 exhibited different effects on the plus-end tracking of EB1, we conducted *in vitro* microtubule assays of EB1 in combination with these CDK5RAP2 fragments. First, microtubule binding was evaluated in a microtubule cosedimentation assay in which the recombinant proteins were incubated with preassembled microtubules. After sedimentation by centrifugation, the distribution of the recombinant proteins between the supernatant and the microtubule pellet was examined. In the absence of EB1, none of M1 or its fragments

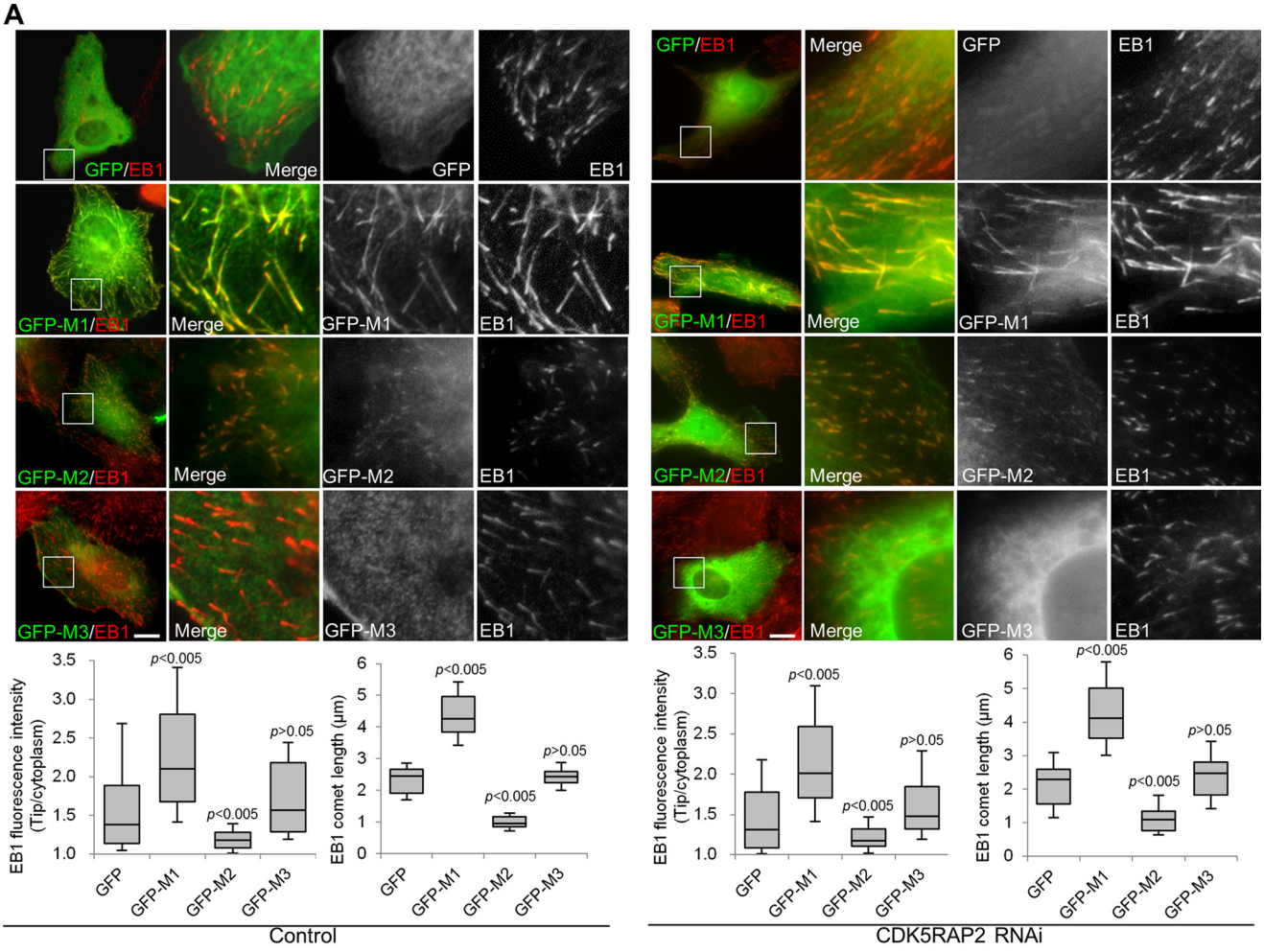

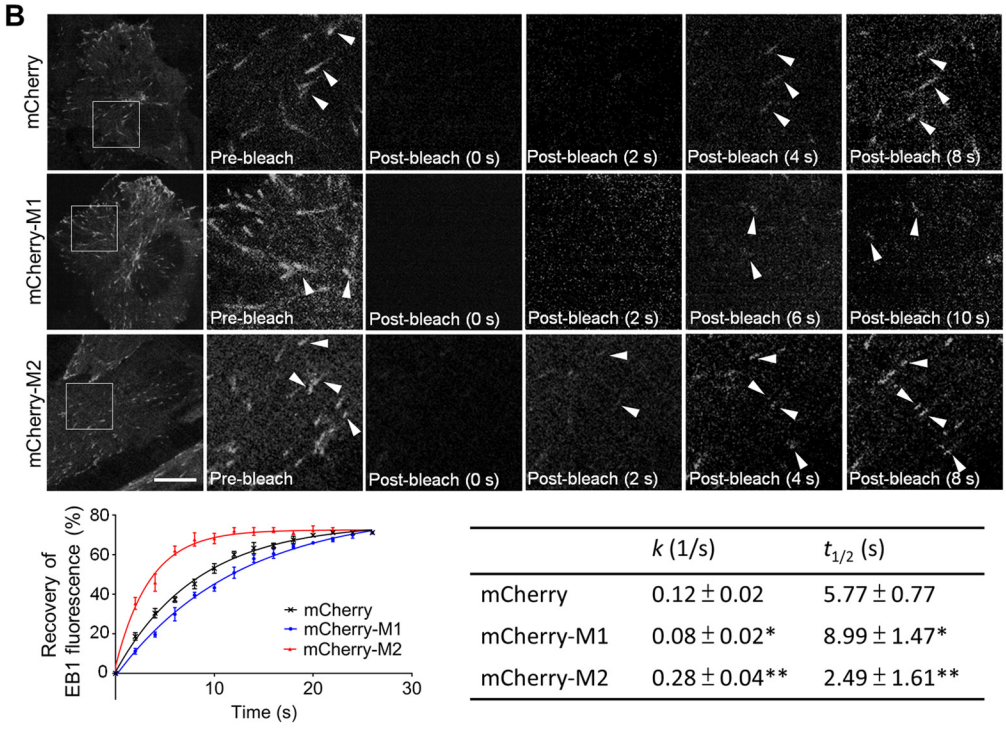

	k (1/s)	$t_{1/2}$ (s)
mCherry	0.12 ± 0.02	5.77 ± 0.77
mCherry-M1	0.08 ± 0.02*	8.99 ± 1.47*
mCherry-M2	0.28 ± 0.04**	2.49 ± 1.61**

cosedimented with microtubules (Fig. 4*A*). The two complexes EB1-M1 and EB1-M2 exhibited similar and strong microtubule-binding activities, whereas the added EB1 and M3 failed to associate with microtubules (Fig. 4*A*). These results revealed that the binding of the S*X*IP sequence stimulates the microtubule-binding activity of EB1 and that dimerization of the S*X*IP sequence is not required for this function.

Second, the potential α/β-tubulin-binding activity of EB1 was tested in a GST pulldown assay. M1 and its fragments did not bind to α/β-tubulin heterodimers without EB1 (data not shown). EB1 pulled down α/β-tubulin heterodimers only in the presence of M1 or M2 but not in the presence of M3 or in the absence of these CDK5RAP2 fragments (Fig. 4*B*). Under the experimental conditions, only the complexes EB1-M1 and EB1-M2 associated with α/β-tubulin heterodimers but not each single protein. In addition, EB1-M1 and EB1-M2 exhibited similar binding activities toward α/β-tubulin heterodimers (Fig. 4*B*), indicating that dimerization of the S*X*IP sequence is not required for the α/β-tubulin binding of its EB1 complex.

Third, we tested the EB1 activity of promoting microtubule polymerization in a light-scattering assay (27). EB1 was applied at a low concentration (0.5 μM) close to the endogenous concentration determined from *Xenopus* eggs (0.27 μM; Ref. 15). At such a low concentration, EB1 free of S*X*IP partners did not induce microtubule polymerization (Fig. 4*C*). Similarly, none of the CDK5RAP2 fragments M1, M2, and M3 alone triggered microtubule polymerization (Fig. 4*C*). However, the combination of EB1 and M1 significantly enhanced light scattering, revealing that the EB1-M1 complex had a strong activity of elongating the microtubule seeds (Fig. 4*C*). These observations agree with previous findings (7). Note that the L938A/P939A mutant of M1 does not have this activity (7). Furthermore, the combination of EB1 and M2 or M3 resulted in minimal increases of light scattering (Fig. 4*C*).

To visualize polymerized microtubules by microscopy, the polymerization assays were performed with a mixture of rhodamine-labeled and -unlabeled α/β-tubulin. Remarkably, the combination of EB1 and M1 promoted the polymerization of longer and more microtubules than EB1 alone or the combination of EB1 and M2 (Fig. 4*D*). Moreover, the inclusion of both EB1 and M1 induced the formation of microtubule bundles (Fig. 4*D*), in agreement with the reported observations (7). By contrast, microtubule bundles were not observed in the assay samples of EB1 alone or EB1 plus M2 (Fig. 4*D*). These results revealed that the S*X*IP dimerization stimulated the microtubule-elongating and bundling activities of the S*X*IP-EB1 complex.

To gain more insight into the mechanism by which CDK5RAP2 regulates EB1, we tested whether M1 promotes the intermolecular self-association of EB1. In a binding assay, the combination of two differentially tagged (His_6-GFP or GST) EB1 proteins was incubated with M1- or the EB1-binding-deficient mutant L938A/P939A. After incubation, anti-GFP immunoprecipitation was performed. Whereas the presence of M1 conferred robust co-immunoprecipitation of GST-EB1 with His_6-GFP-EB1, the inclusion of the L938A/P939A mutant failed to do so (Fig. 4*E*). Therefore, the binding of M1 promotes the intermolecular interaction between EB1 proteins.

Plus-end tracking by CDK5RAP2-APC chimeras

To support the notion that highly active plus-end tracking of the S*X*IP motif requires its dimerization, chimeras were constructed to consist of an S*X*IP sequence and a dimerization domain derived from different +TIPs, CDK5RAP2 and APC. APC contains a dimerization domain and an S*X*IP motif located at the amino- and carboxyl-terminal regions, respectively (6, 9, 28, 29). The chimera M3-APC(C) consists of the dimerization domain from CDK5RAP2 (*i.e.* M3) in fusion with the S*X*IP sequence from APC (*i.e.* 2780–2843 of APC); M2-APC(N) is the chimera of the S*X*IP sequence from CDK5RAP2 (*i.e.* M2) and the dimerization domain from APC (*i.e.* 1–171 of APC). The binding of the chimeras to EB1 was ascertained by their co-immunoprecipitation of EB1; the dimerization domains alone failed to bind to EB1 (Fig. 5*A*).

The intermolecular self-association of the chimeras was examined by immunoprecipitation through the ectopic tag of one construct to detect the co-precipitation of another co-expressed construct. M2-APC(N) interacted with the APC(N)-containing construct but did not bind to the others (Fig. 5*B*). Similarly, M3-APC(C) interacted only with the M3-containing proteins (Fig. 5*B*). Therefore, the chimeras self-associate via their respective dimerization domains. In addition, the self-associations are specific, as the dimerization domain from CDK5RAP2 did not interact with that of APC (Fig. 5*B*).

Next, chimeras and their individual domains were checked if possessing plus-end-tracking activities. APC(C) showed a weak tip-tracking activity, whereas the chimera M3-APC(C) showed an ~2.1-fold stronger activity (Fig. 5, *C* and *E*; supplemental Movies S7 and S8). The weak tracking activity observed in APC(C) is consistent with a previous report (4). M2-APC(N) also showed a dynamic comet-like pattern with the signals enriched at the microtubule plus ends, whereas APC(N) displayed a diffuse pattern without any discernible tracking of the plus ends (Fig. 5, *D* and *E*; supplemental Movies S9 and S10). Notably, the tip-tracking activity of M2-APC(N) was ~3.5-fold stronger than that of M2 (Figs. 1*B* and 5*E*). The addition of a dimerization domain significantly enhanced the tip-tracking activity of the S*X*IP sequences.

Figure 2. Effects of M1 and its fragments on the plus-end tracking of EB1. *A*, GFP and GFP-tagged CDK5RAP2 fragments were transiently expressed in control U2OS cells and in U2OS cells that were depleted of CDK5RAP2 by RNAi. The cells were stained using an anti-EB1 antibody. *Boxed areas* are enlarged. The fluorescence intensities and the comet lengths of EB1 were measured at the microtubule distal tips and in the cytoplasm. The microtubule tip/cytoplasm ratios are determined from 100 microtubule tips from 10 cells that expressed the CDK5RAP2 fragments at low levels. In the *box-and-whisker plots*, *boxes* represent the 25th and 75th percentiles, a *line within the boxes* depicts the median, and *whiskers* represent the 10th and 90th percentiles. *p* values (Student's unpaired two tails *t* test) reflect the significance of differences between GFP and M1 or its fragments. *B*, U2OS cells stably expressing EB1-GFP were transiently transfected with the plasmids encoding mCherry, mCherry-M1, and mCherry-M2. FRAP was performed on the cells, and representative images of EB1-GFP are shown with *boxed areas enlarged*. *Arrowheads* point to individual EB1 comets. Recovery of EB1 fluorescence at the microtubule plus ends was determined, and fluorescence recovery curves were plotted by fitting the FRAP data into a two-phase association equation, and the *k* (1/s) and $t_{1/2}$ (s) corresponding to the slow phase of fluorescent recovery were determined. Data presented are the mean ± S.D. of 40 EB1 comets selected from 10 cells for each construct. *Bars*, 10 μm.

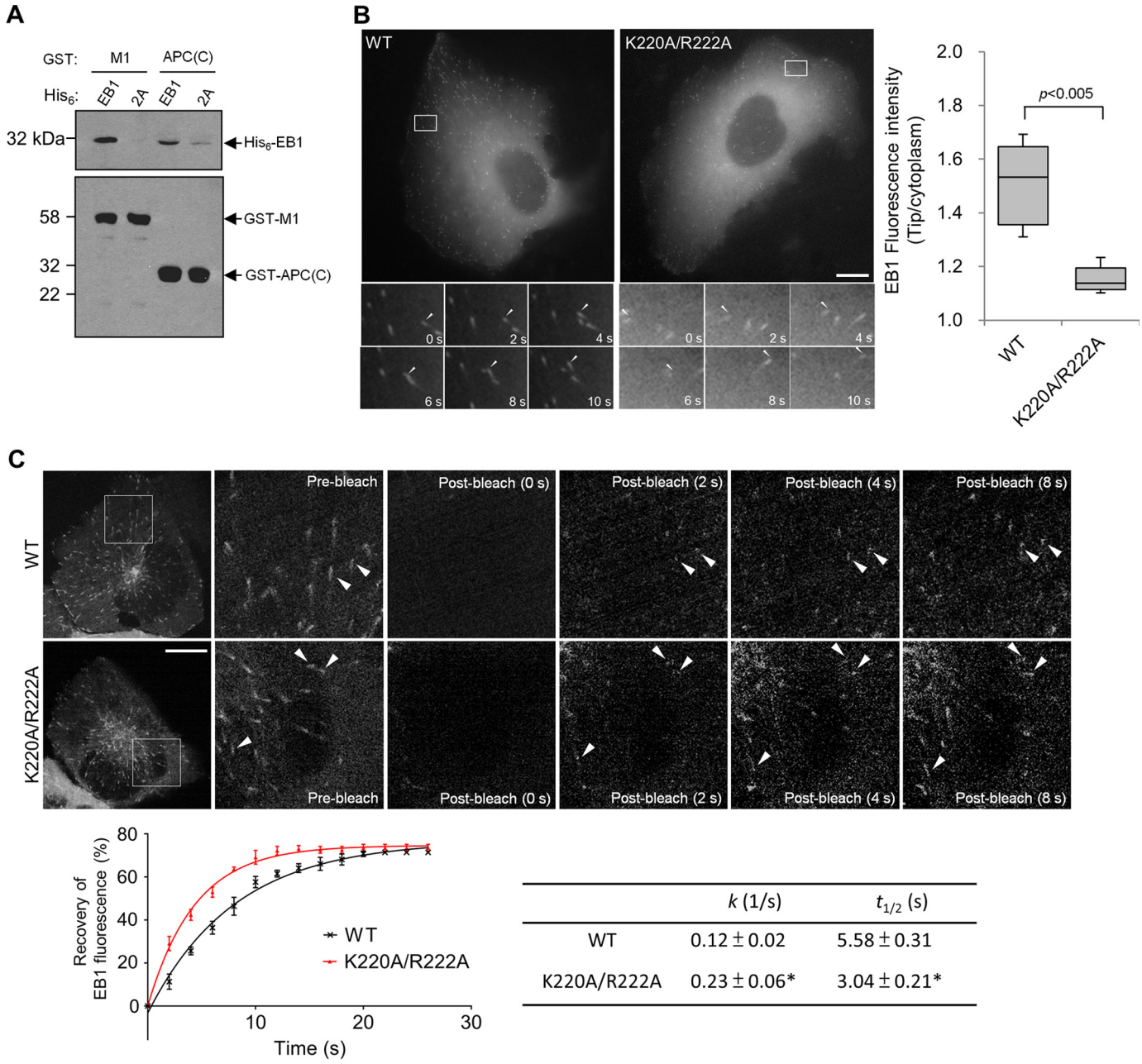

	k (1/s)	$t_{1/2}$ (s)
WT	0.12 ± 0.02	5.58 ± 0.31
K220A/R222A	0.23 ± 0.06*	3.04 ± 0.21*

Figure 3. Plus-end tracking by EB1 and its mutant. *A*, His_6-EB1 and its K220A/R222A mutant (*2A*) were tested in an *in vitro* binding assay with GST-M1 and GST-APC(C), and each recombinant protein was used at 0.5 μM. After incubation of the EB1 proteins with the GST proteins, the GST pulldowns were analyzed by means of anti-His_6 and anti-GST immunoblotting (*IB*). Wild-type EB1 was coprecipitated with GST-M1 and GST-APC(C), but the K220A/R222A mutant failed to do so. *B*, EB1 (WT) or the mutant (K220A/R222A) were transiently expressed in fusion with GFP in U2OS cells that were depleted of endogenous EB1 and EB3 by RNAi. The dynamic movement of the EB1 proteins was recorded by time-lapse microscopy from cells expressing the proteins at low levels. Time series of the *boxed areas* are shown below. The tip/cytoplasm intensity ratios of EB1 were determined from 80 microtubule tips of 8 transfected cells for each construct and are presented as *box-and-whisker plots*: *boxes* represent the 25th and 75th percentiles, a *line within the boxes* depicts the median, and *whiskers* represent the 10th and 90th percentiles. $p < 0.005$, unpaired Student's *t* test. Cells expressing EB1-GFP or its mutant at similar levels were chosen for quantification. *C*, U2OS cells transfected as in *B* were subjected to FRAP. Shown are representative images, and the *boxed areas* are enlarged with *arrowheads* pointing to EB1 comets. Fluorescence recovery plots are from the averaged FRAP data of 50 EB1 comets selected from 10 cells for each construct; *k* (1/s) and $t_{1/2}$ (s) values are mean ± S.D. *Bars*, 10 μm.

Inhibitory effect of the dimerization domains

The above results pointed to the idea that disruption of SXIP dimerization interferes with its tracking of microtubule plus ends. To validate this idea, we expressed the dimerization domains M3 and APC(N) and assessed the potential impacts on the tip tracking of the chimeras. The plus-end attachment of M2-APC(N) was reduced significantly (~67% reduction) by APC(N) expression but was unaffected by M3 expression (Fig. 6, *A* and *C*). Similarly, the plus-end accumulation of M3-APC(C) was impaired (~56% reduction) by M3 expression but not by APC(N) expression (Fig. 6, *B* and *C*). These results are consistent with the interaction specificity observed in the dimerization domains (Fig. 5*B*), indicating that the dimerization domains interfere specifically with the plus-end tracking of their parent proteins.

Similar experiments were performed to evaluate the effects of M2 and M3 on M1. The plus-end tracking of M1 was unaf-

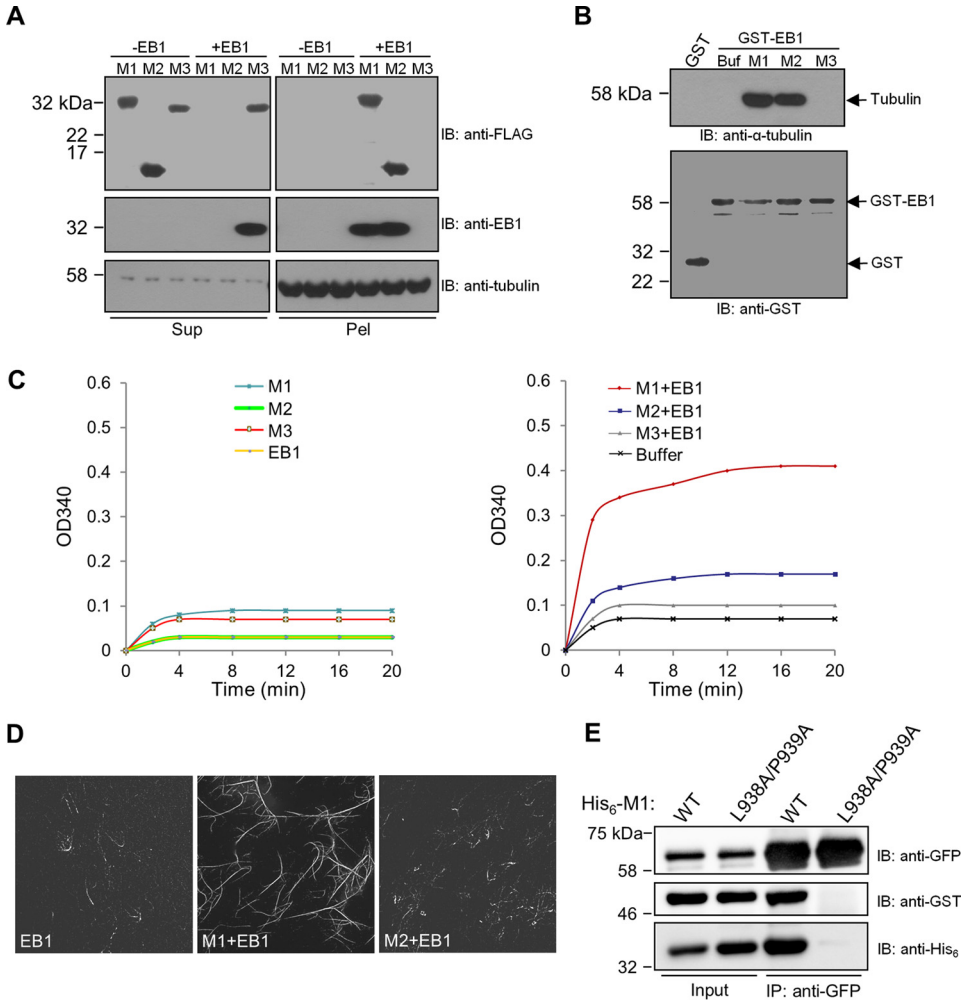

Figure 4. Effects of *SXIP* proteins on EB1 activities toward microtubules and α/β-tubulin and on EB1 dimerization. *A*, a microtubule sedimentation assay was performed with the purified recombinant proteins of CDK5RAP2 fragments and EB1. In the assay, microtubules preassembled from 1 μM α/β-tubulin were incubated with the CDK5RAP2 fragments (His_6-FLAG tagged; 0.5 μM) and EB1 (His_6 tagged; 0.5 μM). After sedimentation, the resulting supernatants (*Sup*) and pellets (*Pel*) were analyzed by immunoblotting (*IB*) as indicated. *B*, the binding of GST and GST-EB1 to α/β-tubulin heterodimers was tested in a GST pulldown assay. α/β-Tubulin heterodimers (1 μM) were incubated with the GST proteins (1 μM) alone and in combination with different CDK5RAP2 fragments (His_6-FLAG tagged; 1.25 μM). *Buf*, Buffer. The GST pulldown samples were analyzed by means of anti-α-tubulin and anti-GST immunoblotting. α/β-Tubulin heterodimers were coprecipitated with GST-EB1 in the presence of M1 or M2 but failed to coprecipitated with GST-EB1 alone or GST-EB1 plus M3. *C*, microtubule polymerization was conducted with α/β-tubulin heterodimers (18 μM) and microtubule seeds (0.1 μg/μl). The recombinant proteins of M1, M2, M3, and EB1 (0.5 μM) were applied alone or in combinations. *D*, microtubules were polymerized from a mixture of rhodamine-labeled and unlabeled α/β-tubulin as in *C*. The polymerized microtubules were examined by fluorescence microscopy. *E*, in a binding assay of purified recombinant proteins, His_6-GFP-EB1 (0.09 μM) was incubated with GST-EB1 (0.16 μM) in the presence of wild-type His_6-M1 (*WT*) or His_6-M1(*L938A/P939A*) (2.5 μM). After anti-GFP immunoprecipitation (*IP*), the immunoprecipitates (50%) and the protein inputs (2%) were analyzed by means of immunoblotting. GST-EB1 was coprecipitated with His_6-GFP-EB1 in the presence of wild-type M1 but not in the presence of the mutant.

fected by the expression of GFP, which was the ectopic tag of the M2 and M3 constructs (Fig. 7, *A* and *B*). The M2 expression ablated the accumulation of M1 at the microtubule plus ends (Fig. 7, *A* and *B*), which is consistent with the disruption of M1-EB1 interaction by the overexpressed M2. More interestingly, M3 expression significantly reduced but did not eliminate the tip-tracking behavior of M1 (Fig. 7, *A* and *B*). Therefore, dimerization of the *SXIP* sequence is required for highly active tracking of microtubule plus ends.

Previous studies have shown that the expression of the amino-terminal fragments of APC that lack the EB1-binding domain affects the function of EB1 at microtubule plus ends and causes defects in kinetochore-microtubule interactions (30–32). Because these fragments contain the dimerization domain, our results suggested that the expressions impair the plus-end-associated functions of intact APC. We then overexpressed the dimerization domain APC(N) and checked its potential effect on chromatin structure. In comparison, the dimerization domain of CDK5RAP2 (*i.e.* M3) was expressed. The APC(N) expression caused the deformation of chromatin in a large population of transfected cells, whereas M3 expression did not give rise to such an effect (Fig. 8). These results further revealed the specificity of the actions exerted by the dimerization domains.

Discussion

EBs play a central role in the assembly of protein complexes associated with microtubule plus ends. Notably, a functionally diverse group of proteins contains the *SXIP* motif for binding with EBs and, thus, for plus-end tracking (1, 2, 4). To further

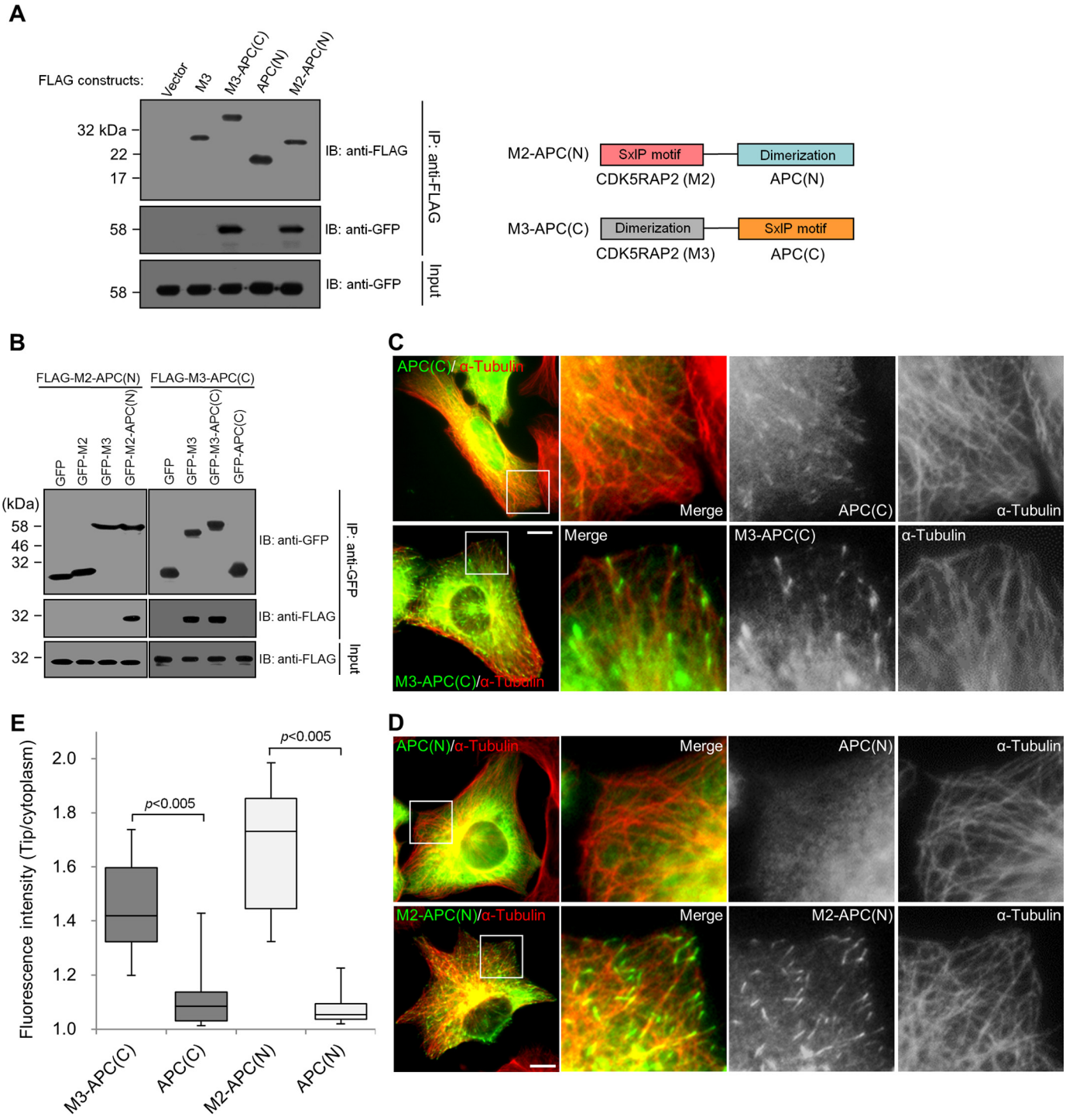

Figure 5. Construction of plus-end-tracking chimeras. *A*, the chimeras and the single domains of CDK5RAP2 and APC were transiently expressed as FLAG-tagged proteins, and EB1-GFP was co-expressed in HEK293T cells. After anti-FLAG immunoprecipitation (*IP*), the immunoprecipitates and the lysate inputs were analyzed by means of immunoblotting (*IB*). EB1-GFP was co-immunoprecipitated with the chimeras M3-APC(C) and M2-APC(N) but not with the dimerization domains APC(N) and M3 only. *Right*, a schematic representation of the chimeras. *B*, the extracts of HEK293T cells co-expressing the GFP-tagged and the FLAG-tagged proteins as indicated were subjected to anti-GFP immunoprecipitation (*IP*). The immunoprecipitates and the lysate inputs were analyzed by means of anti-GFP and anti-FLAG immunoblotting (*IB*). M2-APC(N) was coprecipitated only with the APC(N)-containing construct, whereas M3-APC(C) was coprecipitated only with the M3-containing constructs. *C* and *D*, U2OS cells were transiently transfected with FLAG-tagged APC(C), M3-APC(C), APC(N), or M2-APC(N). The cells were stained for the ectopically expressed proteins (anti-FLAG) and microtubules (anti-α-tubulin). *Boxed areas* are enlarged. *Bars*, 10 μm. *E*, the immunofluorescence signals of the proteins expressed at similar levels in *C* and *D* were quantified from 50 microtubule tips in 5 transfected cells to derive the microtubule tip/cytoplasm ratios. Data are presented in the same *box-and-whisker* format as in Fig. 1: *boxes* represent the 25th and 75th percentiles, a *line within the boxes* depicts the median, and *whiskers* represent the 10th and 90th percentiles. *p* values were calculated by the Student's unpaired two tails *t* test.

understand the plus-end tracking of EB-SXIP complexes, we dissected the plus-end-tracking module of CDK5RAP2 and analyzed the SXIP impacts on EB1 activities using *in vivo* and *in vitro* assays. The results have demonstrated that CDK5RAP2, and perhaps other SXIP-containing +TIPs, exerts a regulatory role on their bound EB1 for tracking of growing microtubule

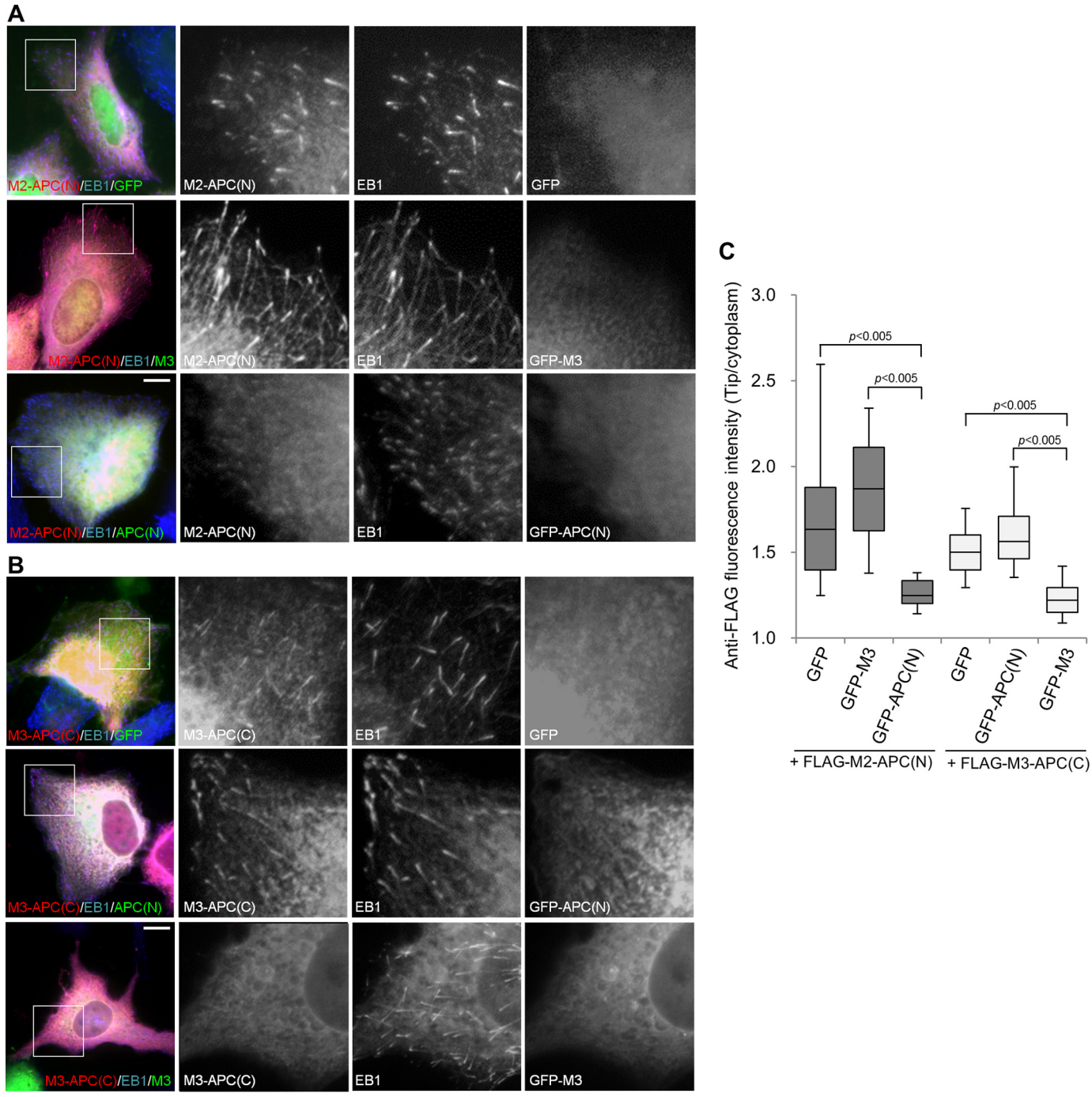

Figure 6. Disruption of SXIP dimerization interferes with microtubule plus-end tracking. *A*, U2OS cells were transiently cotransfected with plasmids encoding FLAG-M2-APC(N) and a GFP fusion protein (GFP, GFP-M3, or GFP-APC(N)). The cells were stained with anti-FLAG and anti-EB1 antibodies. *B*, FLAG-M3-APC(C) was transiently co-expressed with GFP, GFP-APC(N), or GFP-M3 in U2OS cells. *A* and *B*, *boxed areas* are enlarged. *Bars*, 10 μm. *C*, the intensities of anti-FLAG immunofluorescence were measured at microtubule tips as labeled by anti-EB1 staining and in the cytoplasm. In each group, 80–100 microtubule tips were measured from 8–10 cells that expressed the FLAG-tagged proteins and the GFP proteins at low and moderate levels, respectively. In the *box-and-whisker plots*, *boxes* represent the 25th and 75th percentiles, a *line within the boxes* depicts the median, and whiskers represent the 10th and 90th percentiles. The significance of differences between the indicated values was evaluated by Student's unpaired two-tailed *t* test.

tips. Furthermore, we revealed the role of the dimerization/multimerization of the SXIP sequences in tracking microtubule tips.

Although EB1 possesses an intrinsic plus-end-tracking activity (3), our results indicate that its activity is altered upon binding to the SXIP sequence of CDK5RAP2; that is, the plus-end tracking of EB1 is significantly augmented, and the dynamic exchange of EB1 is reduced at microtubule plus ends by the dimerization/multimerization of the bound SXIP sequence. These findings are in line with the previous observations that either the depletion of APC or the expression of an amino-terminal fragment of APC, which dimerizes with endogenous APC without binding to EB1, reduces EB1 signals at the plus ends (31). Therefore, a highly active SXIP-EB1 complex re-

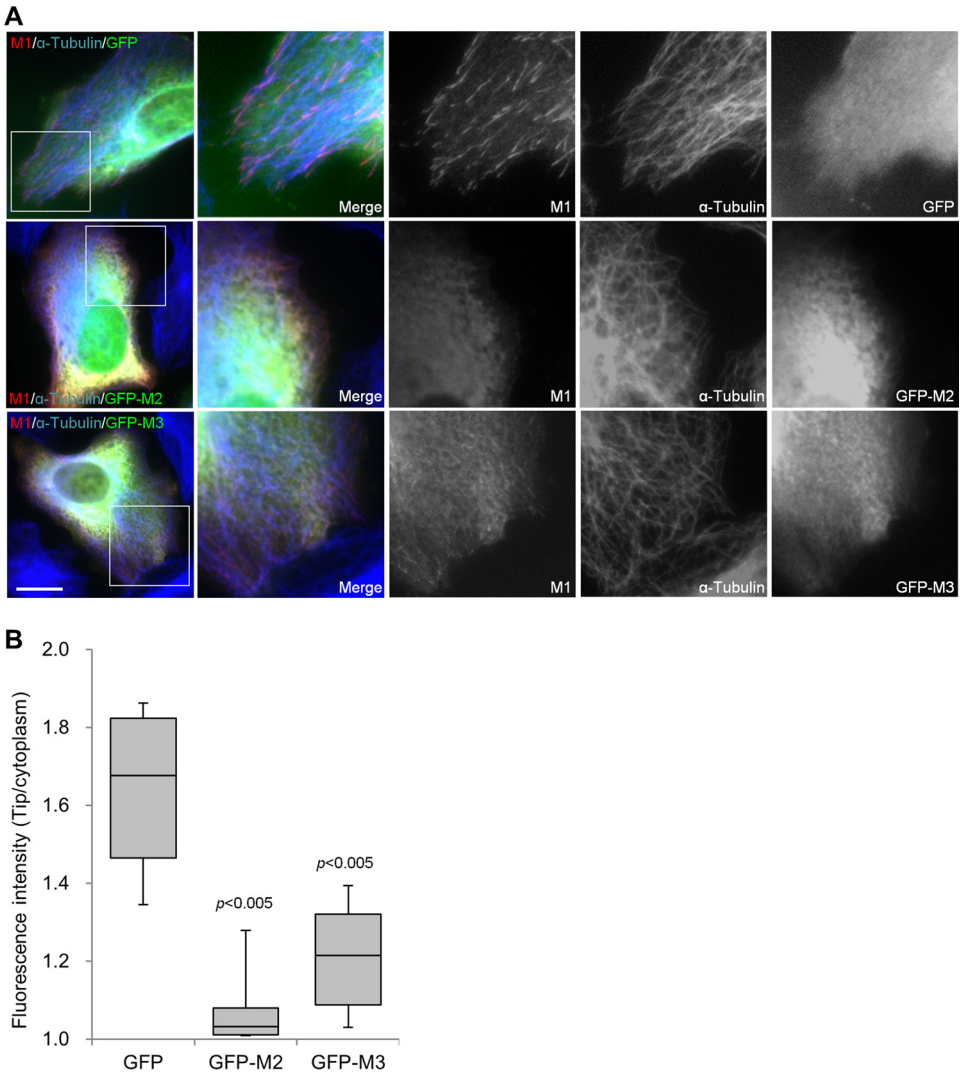

Figure 7. M2 and M3 interfere with the plus-end tracking of M1. *A*, FLAG-M1 was transiently co-expressed in U2OS cells with GFP, GFP-M2, or GFP-M3. The cells were stained with anti-FLAG and anti-α-tubulin antibodies. *Boxed areas* are enlarged. *Bar*, 10 μm. *B*, the fluorescence intensities of M1 were acquired at the microtubule distal tips and in the cytoplasm in five transfected cells that expressed FLAG-M1 and the GFP proteins at low and moderate levels, respectively. The intensity ratios (tip/cytoplasm) are presented as *box-and-whisker plots* in which *boxes* represent the 25th and 75th percentiles, a *line within the boxes* depicts the median, and *whiskers* represent the 10th and 90th percentiles. *p* values (Student's unpaired two-tailed *t* test) indicate the significance of differences between GFP and GFP-M2 or GFP-M3.

quires the S*X*IP protein that contains a dimerization domain. Alternatively, an S*X*IP module may have high tracking activity by containing multiple S*X*IP sequences instead of dimerization domains within the protein. In fact, +TIPs are often found to contain dimerization domains and/or multiple EB1-binding regions (1, 2, 4).

We further explored the effects of S*X*IP dimerization/multimerization on its bound EB1. Under the experimental conditions of our co-immunoprecipitation, we did not detect any effect of S*X*IP dimerization/multimerization on its EB1 binding (Fig. 1*A*). However, S*X*IP dimerization/multimerization promoted the intermolecular self-association of its bound EB1 (Fig. 4*D*). Although monomeric EB1 tracks growing microtubule plus ends, EB1 dimerization is required for its anti-catastrophe activity (16). At physiological concentrations, most EB1 proteins exist as a homodimer or as a heterodimer with EB3, and the dimerization is regulated by binding of GTP (24, 33–36). However, it is unclear whether EB1 forms multimeric complexes. Our results suggested that the dimerization/multimerization of the S*X*IP from CDK5RAP2 allows the bound EB1 proteins to form larger multimeric complexes, promoting the accumulation of EB1 and the S*X*IP protein at growing plus ends. Beyond this, the binding to the dimeric/multimeric S*X*IP sequence (*i.e.* M1) but not to the single S*X*IP sequence (*i.e.* M2) significantly enhanced the microtubule-elongating and bundling activities of EB1 (Fig. 7*D*). Because the comet tail length of EB1 shows strong dependence on the growth rate of microtubules (3, 37), the dimerization/multimerization of the S*X*IP sequence may facilitate the attachment of EB1-S*X*IP to growing plus ends by promoting microtubule assembly. We conclude that EB1 cooperates with its bound S*X*IP proteins for tracking growing microtubule tips.

EB1 or its homologs recognize the GTP structural cap of growing microtubule plus ends, and the binding is located at the interface of four adjacent α/β-tubulin heterodimers in the microtubule lattice (38, 39). Furthermore, EB1 alone does not

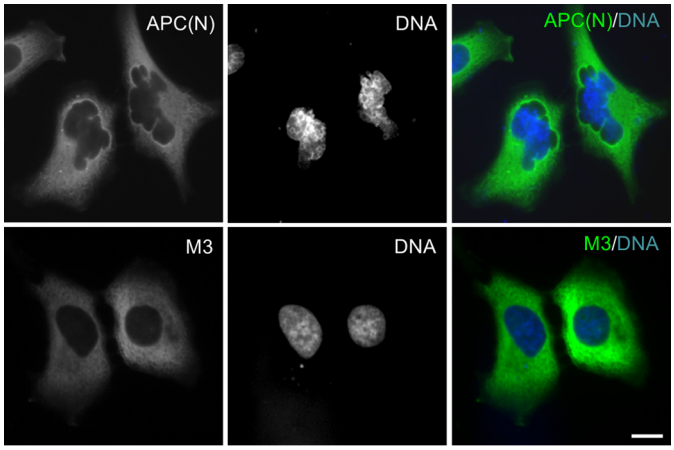

Figure 8. Expression of APC(N) but not M3 results in chromatin deformation. U2OS cells were transiently transfected with GFP-APC(N) or GFP-M3. Nuclear DNA was labeled with Hoechst 33258. Chromatin deformation was observed in 56% of GFP-APC(N)-transfected cells ($n = 103$) and only 14% of GFP-M3-transfected cells showed defects in nuclear morphology ($n = 100$). *Bar*, 10 μM.

bind to α/β-tubulin dimers (40, 41). We observed that not only the microtubule-binding activity but also the α/β-tubulin-binding activity was stimulated upon its binding to the S*X*IP motif of CDK5RAP2 (Fig. 4, *A–B*). Similar observations have been reported for the association of EB1 with the CAP-Gly domain-containing cytoplasmic linker protein CLIP-170; the binding promotes the α/β-tubulin binding and plus-end recruitment of EB1 (41). Therefore, EB1 may require binding to either an S*X*IP protein or a CAP-Gly protein for highly active microtubule plus-end tracking. Because EB1 interacts with a multitude of +TIPs (42), it is conceivable that EB1 displays various tip-tracking activities by interacting with different +TIPs.

The present study has also shown that the dimerization domain of S*X*IP proteins can be used to delocalize individual S*X*IP proteins from microtubule plus ends. Obviously, the binding specificity of the dimerization domains is key to such applications. The dimerization domains of CDK5RAP2 (*i.e.* M3) and APC, *i.e.* APC(N), did not bind to each other (Fig. 3*B*). In addition, these dimerization domains delocalized their respective tip-tracking chimeras from microtubule tips without affecting the tip attachment of the others (Fig. 4). Therefore, we propose that the dimerization domains provide tools to investigate the plus-end-associated function of individual S*X*IP proteins. Indeed, the expression of the dimerization domain in APC but not that in CDK5RAP2 compromised the plus-end-associated functions of APC and caused chromatin deformation (Fig. 8; Refs. 27–29).

Chromatin deformation has been observed in U2OS cells depleted of APC as a consequence of chromosome instability (43). In *APC*-defective colorectal tumors, APC mutations generate their carboxyl-terminal-truncated proteins, which are believed to induce chromosome instability and, consequently, tumorigenesis in a dominant manner (44, 45). By dimerizing with intact APC, these truncation fragments interfere with the plus-end localization of APC as well as its bound EB1, and thus act as dominant inhibitory species. Indeed, the dimerization domain at the amino terminus is required for the observed dominant effects (31).

Overall, an important finding of the present study is that CDK5RAP2 and perhaps other S*X*IP-containing proteins regulate the tip-tracking activity of their bound EB1 instead of passively hitchhiking on EB1. To form a highly active tip-tracking module, the S*X*IP motif requires a dimerization domain in addition to binding to EB1. Because the attachment to growing microtubule tips enables +TIPs to exert their actions in a wide variety of microtubule-mediated processes, including mitotic chromosome segregation, cell polarization, migration and morphogenesis, the present work raises the interesting possibility that disruption of the dimerization/multimerization of S*X*IP proteins serves as an approach to specifically explore the microtubule tip-associated functions of individual S*X*IP proteins. Moreover, the expression of an S*X*IP-containing sequence without any dimerization domain would block the binding of S*X*IP proteins to EB1, acting as a dominant-negative species nondiscriminative to all S*X*IP proteins. Taken together, our findings provide a better understanding on the mechanism by which EB1-S*X*IP protein complexes track growing microtubule tips.

Experimental procedures

Reagents

The chimeras of CDK5RAP2 and APC were generated using polymerase chain reaction-based methods. The following reagents used have been reported previously: CDK5RAP2 expression constructs and antibodies and mCherry-α-tubulin (7, 19). The recombinant proteins of CDK5RAP2 fragments and EB1 were prepared by bacterial expression and affinity purification (7). A siRNA duplex was synthesized to target the 3′-untranslated region of *eb1* (5′-GGAGAAAUGUAAAGACUGA-3′); a siRNA oligonucleotide duplex against *eb3* (5′-ACUAUGAUGGAAAGGAUUAC-3′) was used as previously reported (7, 25). The siRNA duplex against human *cdk5rap2* (5′-UGGAAGAUCUCCUAACUAA-3′) was used as described (19). Antibodies purchased were anti-EB1 (BD Biosciences), anti-EB3 (KT53, Thermo Scientific), anti-FLAG (monoclonal M2 and polyclonal, Sigma), anti-α-tubulin (B-5–1-2, Sigma), anti-GST (B-14, Santa Cruz Biotechnology), anti-His_6 (H-15, Santa Cruz Biotechnology), and anti-GFP (FL, Santa Cruz Biotechnology).

Protein binding assays

To prepare for immunoprecipitation, cells were extracted in protein binding buffer (25 mM Tris-HCl, pH 7.4, 0.5% IGEPAL CA-630, 100 mM NaCl, 5 mM $MgCl_2$, 5 mM NaF, 20 mM β-glycerophosphate, 1 mM dithiothreitol, 1 mM EDTA, and Complete Protease Inhibitor Mixture (Roche Applied Science)). The extracts were then clarified by centrifugation at 4 °C in a microcentrifuge. Immunoprecipitation was performed with anti-FLAG M2-coupled beads (Sigma) or antibodies coupled to Protein A/G-agarose (Invitrogen); immunoprecipitates were examined on immunoblots.

Protein *in vitro* binding assays were conducted in protein binding buffer using recombinant proteins. In the α/β-tubulin-binding assay, the binding buffer was supplemented with 0.1 mM GTP. After binding (1 h, 4 °C), GST fusion proteins were

retrieved using GSH-Sepharose (GE Healthcare), and the pull-downs were examined by SDS-PAGE and immunoblotting.

Immunofluorescence and time-lapse microscopy

HEK293T and U2OS were cultured at 37 °C in 5% CO_2 in DMEM plus 10% fetal bovine serum (Invitrogen). To perform immunofluorescence imaging, cells grown on coverslips were fixed either in methanol (10 min, −20 °C) or in 4% paraformaldehyde in phosphate-buffered saline (15 min, room temperature). Fluorescence images were obtained using a Nikon microscope (Eclipse TE2000) equipped with the camera SPOT RT1200 (Diagnostic Instruments) or a Carl Zeiss microscope (Axio Observer Z1) equipped with an sCMOS camera (ORCA-FLASH4.0, Hamamatsu). In experiments using transiently transfected cells, we imaged the cells that expressed the transfected constructs at low to moderate levels. To determine the amount of proteins at microtubule distal tips relative to that in the cytoplasm, fluorescence intensities were measured from a rectangular area covering the entire tip (8 × 30 pixels) and also from a cytoplasmic area of same size (7). After background subtraction, the intensity ratios of microtubule tip over cytoplasm were calculated.

Time-lapse microscopy was conducted on cells grown on 35-mm glass-bottom dishes. Images were collected on a Nikon microscope (Eclipse TE2000) equipped with an EMCCD camera (SPOT BOOST BT2100, Diagnostic Instruments) and an incubation chamber to maintain the culture conditions. TIF image stacks were exported as MOV files using the MetaMorph software. The play-back rate is 5 frames/s.

FRAP assay

Cells grown on 25-mm coverslips were imaged using a spinning disk confocal microscope (Axio Observer ZI, Carl Zeiss; Revolution XDi Laser-based Spinning Disk System, Andor). Culture conditions were maintained in a stage-top incubator (Chamlide). FRAP was performed using a FRAP bleaching device (FRAPPA, Andor), and time-lapse images were acquired at every 2 s using a Neo sCMOS camera (Andor). The image stacks were processed and exported using the FIJI package of ImageJ (46). The fluorescence intensity of EB1 at microtubule distal tips was quantified. After normalization by the intensity in the cytoplasm, the data were used to determine fluorescence recoveries (ratios of post- and prephotobleaching intensities), and the average fluorescence recoveries at various time points were fitted into a two-phase association equation (GraphPad Prism, GraphPad Software), $y = y_0 + \text{Span}_{\text{Fast}} \times (1 - \exp(-k_{\text{Fast}} \times x)) + \text{Span}_{\text{Slow}} \times (1 - \exp(-k_{\text{Slow}} \times x))$, where $\text{Span}_{\text{Fast}} = (\text{plateau} - y_0) \times \text{Percent}_{\text{Fast}} \times 0.01$ and $\text{Span}_{\text{Slow}} = (\text{plateau} - y_0) \times (100 - \text{Percent}_{\text{Fast}}) \times 0.01$. k_{slow} (1/s) and $t_{½}$ (s) were determined from the slow phase of fluorescence recovery curves.

Microtubule assays

To test microtubule binding, microtubules were preassembled at 37 °C for 30 min from purified porcine-brain α/β-tubulin (27) in PEM buffer (80 mM PIPES, pH 6.8, 1 mM $MgCl_2$, and 1 mM EGTA) supplemented with 40 μM taxol and 1 mM GTP. The binding assays were conducted with the microtubules in the taxol-containing buffer at room temperature for 30 min. After binding, the samples were centrifuged at 100,000 × *g* for 15 min over a sucrose cushion (25% w/v) in PEM buffer; the resulting pellets and supernatants were analyzed by immunoblotting.

Microtubule polymerization was analyzed in a light-scattering assay using α/β-tubulin (18 μM) and 0.1 μg/μl microtubule seeds (7), which were prepared by shearing taxol-stabilized microtubules through a 26-gauge needle. To visualize polymerized microtubules, rhodamine-labeled (Cytoskeleton, Inc.) and unlabeled α/β-tubulin were premixed at the ratio of 1:20 for polymerization (7). Polymerized microtubules were fixed in 0.5% glutaraldehyde and then visualized by fluorescence microscopy.

Author contributions—K.-W. F., F. K. C. A., Y. J., S. Y., and R. Z. Q. designed the experiments. K.-W. F., F. K. C. A., Y. J., S. Y., and L. Z. conducted the experiments. K.-W.F., F. K. C. A., Y. J., S. Y., L.Z., and R. Z. Q. analyzed the data. K.-W. F., F. K. C. A., and R. Z. Q. wrote the paper.

Acknowledgment—We thank Dr. Xiang Yu (Institute of Neuroscience, China) for an APC construct.

References

1. Akhmanova, A., and Steinmetz, M. O. (2008) Tracking the ends: a dynamic protein network controls the fate of microtubule tips. *Nat. Rev. Mol. Cell Biol.* **9,** 309–322
2. Akhmanova, A., and Steinmetz, M. O. (2015) Control of microtubule organization and dynamics: two ends in the limelight. *Nat. Rev. Mol. Cell Biol.* **16,** 711–726
3. Bieling, P., Laan, L., Schek, H., Munteanu, E. L., Sandblad, L., Dogterom, M., Brunner, D., and Surrey, T. (2007) Reconstitution of a microtubule plus-end tracking system *in vitro*. *Nature* **450,** 1100–1105
4. Honnappa, S., Gouveia, S. M., Weisbrich, A., Damberger, F. F., Bhavesh, N. S., Jawhari, H., Grigoriev, I., van Rijssel, F. J., Buey, R. M., Lawera, A., Jelesarov, I., Winkler, F. K., Wüthrich, K., Akhmanova, A., and Steinmetz, M. O. (2009) An EB1-binding motif acts as a microtubule tip localization signal. *Cell* **138,** 366–376
5. Galjart, N. (2005) CLIPs and CLASPs and cellular dynamics. *Nat. Rev. Mol. Cell Biol.* **6,** 487–498
6. Slep, K. C., Rogers, S. L., Elliott, S. L., Ohkura, H., Kolodziej, P. A., and Vale, R. D. (2005) Structural determinants for EB1-mediated recruitment of APC and spectraplakins to the microtubule plus end. *J. Cell Biol.* **168,** 587–598
7. Fong, K.-W., Hau, S.-Y., Kho, Y.-S., Jia, Y., He, L., and Qi, R. Z. (2009) Interaction of CDK5RAP2 with EB1 to track growing microtubule tips and to regulate microtubule dynamics. *Mol. Biol. Cell* **20,** 3660–3670
8. Vaughan, K. T. (2005) TIP maker and TIP marker; EB1 as a master controller of microtubule plus ends. *J. Cell Biol.* **171,** 197–200
9. Bu, W., and Su, L.-K. (2003) Characterization of functional domains of human EB1 family proteins. *J. Biol. Chem.* **278,** 49721–49731
10. Hayashi, I., and Ikura, M. (2003) Crystal structure of the amino-terminal microtubule-binding domain of end-binding protein 1 (EB1). *J. Biol. Chem.* **278,** 36430–36434
11. Hayashi, I., Wilde, A., Mal, T. K., and Ikura, M. (2005) Structural basis for the activation of microtubule assembly by the EB1 and p150Glued complex. *Mol. Cell* **19,** 449–460
12. Honnappa, S., John, C. M., Kostrewa, D., Winkler, F. K., and Steinmetz, M. O. (2005) Structural insights into the EB1-APC interaction. *EMBO J.* **24,** 261–269
13. Ligon, L. A., Shelly, S. S., Tokito, M., and Holzbaur, E. L. (2003) The microtubule plus-end proteins EB1 and dynactin have differential effects on microtubule polymerization. *Mol. Biol. Cell* **14,** 1405–1417

14. Rogers, S. L., Rogers, G. C., Sharp, D. J., and Vale, R. D. (2002) *Drosophila* EB1 is important for proper assembly, dynamics, and positioning of the mitotic spindle. *J. Cell Biol.* **158,** 873–884
15. Tirnauer, J. S., Grego, S., Salmon, E. D., and Mitchison, T. J. (2002) EB1-microtubule interactions in *Xenopus* egg extracts: role of EB1 in microtubule stabilization and mechanisms of targeting to microtubules. *Mol. Biol. Cell* **13,** 3614–3626
16. Komarova, Y., De Groot, C. O., Grigoriev, I., Gouveia, S. M., Munteanu, E. L., Schober, J. M., Honnappa, S., Buey, R. M., Hoogenraad, C. C., Dogterom, M., Borisy, G. G., Steinmetz, M. O., and Akhmanova, A. (2009) Mammalian end binding proteins control persistent microtubule growth. *J. Cell Biol.* **184,** 691–706
17. Vitre, B., Coquelle, F. M., Heichette, C., Garnier, C., Chrétien, D., and Arnal, I. (2008) EB1 regulates microtubule dynamics and tubulin sheet closure *in vitro*. *Nat. Cell Biol.* **10,** 415–421
18. Nakamura, M., Zhou, X. Z., and Lu, K. P. (2001) Critical role for the EB1 and APC interaction in the regulation of microtubule polymerization. *Curr. Biol.* **11,** 1062–1067
19. Fong, K.-W., Choi, Y.-K., Rattner, J. B., and Qi, R. Z. (2008) CDK5RAP2 is a pericentriolar protein that functions in centrosomal attachment of the γ-tubulin ring complex. *Mol. Biol. Cell* **19,** 115–125
20. Choi, Y.-K., Liu, P., Sze, S. K., Dai, C., and Qi, R. Z. (2010) CDK5RAP2 stimulates microtubule nucleation by the γ-tubulin ring complex. *J. Cell Biol.* **191,** 1089–1095
21. Dragestein, K. A., van Cappellen, W. A., van Haren, J., Tsibidis, G. D., Akhmanova, A., Knoch, T. A., Grosveld, F., and Galjart, N. (2008) Dynamic behavior of GFP-CLIP-170 reveals fast protein turnover on microtubule plus ends. *J. Cell Biol.* **180,** 729–737
22. Tortosa, E., Galjart, N., Avila, J., and Sayas, C. L. (2013) MAP1B regulates microtubule dynamics by sequestering EB1/3 in the cytosol of developing neuronal cells. *EMBO J.* **32,** 1293–1306
23. Wen, Y., Eng, C. H., Schmoranzer, J., Cabrera-Poch, N., Morris, E. J., Chen, M., Wallar, B. J., Alberts, A. S., and Gundersen, G. G. (2004) EB1 and APC bind to mDia to stabilize microtubules downstream of Rho and promote cell migration. *Nat. Cell Biol.* **6,** 820–830
24. De Groot, C. O., Jelesarov, I., Damberger, F. F., Bjelić, S., Schärer, M. A., Bhavesh, N. S., Grigoriev, I., Buey, R. M., Wüthrich, K., Capitani, G., Akhmanova, A., and Steinmetz, M. O. (2010) Molecular insights into mammalian end-binding protein heterodimerization. *J. Biol. Chem.* **285,** 5802–5814
25. Komarova, Y., Lansbergen, G., Galjart, N., Grosveld, F., Borisy, G. G., and Akhmanova, A. (2005) EB1 and EB3 control CLIP dissociation from the ends of growing microtubules. *Mol. Biol. Cell* **16,** 5334–5345
26. Honnappa, S., Okhrimenko, O., Jaussi, R., Jawhari, H., Jelesarov, I., Winkler, F. K., and Steinmetz, M. O. (2006) Key interaction modes of dynamic +TIP networks. *Mol. Cell* **23,** 663–671
27. Hou, Z., Li, Q., He, L., Lim, H.-Y., Fu, X., Cheung, N. S., Qi, D. X., and Qi, R. Z. (2007) Microtubule association of the neuronal p35 activator of Cdk5. *J. Biol. Chem.* **282,** 18666–18670
28. Joslyn, G., Richardson, D. S., White, R., and Alber, T. (1993) Dimer formation by an N-terminal coiled coil in the APC protein. *Proc. Natl. Acad. Sci. U.S.A.* **90,** 11109–11113
29. Su, L. K., Johnson, K. A., Smith, K. J., Hill, D. E., Vogelstein, B., and Kinzler, K. W. (1993) Association between wild type and mutant APC gene products. *Cancer Res.* **53,** 2728–2731
30. Green, R. A., and Kaplan, K. B. (2003) Chromosome instability in colorectal tumor cells is associated with defects in microtubule plus-end attachments caused by a dominant mutation in APC. *J. Cell Biol.* **163,** 949–961
31. Green, R. A., Wollman, R., and Kaplan, K. B. (2005) APC and EB1 function together in mitosis to regulate spindle dynamics and chromosome alignment. *Mol. Biol. Cell* **16,** 4609–4622
32. Tighe, A., Johnson, V. L., and Taylor, S. S. (2004) Truncating APC mutations have dominant effects on proliferation, spindle checkpoint control, survival and chromosome stability. *J. Cell Sci.* **117,** 6339–6353
33. Alberico, E. O., Lyons, D. F., Murphy, R. J., Philip, J. T., Duan, A. R., Correia, J. J., and Goodson, H. V. (2013) Biochemical evidence that human EB1 does not bind preferentially to the microtubule seam. *Cytoskeleton* **70,** 317–327
34. Sen, I., Veprintsev, D., Akhmanova, A., and Steinmetz, M. O. (2013) End binding proteins are obligatory dimers. *PloS ONE* **8,** e74448
35. Gireesh, K. K., Sreeja, J. S., Chakraborti, S., Singh, P., Thomas, G. E., Gupta, H., and Manna, T. (2014) Microtubule +TIP protein EB1 binds to GTP and undergoes dissociation from dimer to monomer on binding GTP. *Biochemistry* **53,** 5551–5557
36. Seetapun, D., and Odde, D. J. (2010) Cell-length-dependent microtubule accumulation during polarization. *Curr. Biol.* **20,** 979–988
37. Mimori-Kiyosue, Y., Shiina, N., and Tsukita, S. (2000) Adenomatous polyposis coli (APC) protein moves along microtubules and concentrates at their growing ends in epithelial cells. *J. Cell Biol.* **148,** 505–518
38. Maurer, S. P., Fourniol, F. J., Bohner, G., Moores, C. A., and Surrey, T. (2012) EBs recognize a nucleotide-dependent structural cap at growing microtubule ends. *Cell* **149,** 371–382
39. Zhang, R., Alushin, G. M., Brown, A., and Nogales, E. (2015) Mechanistic origin of microtubule dynamic instability and its modulation by EB proteins. *Cell* **162,** 849–859
40. Slep, K. C., and Vale, R. D. (2007) Structural basis of microtubule plus end tracking by XMAP215, CLIP-170, and EB1. *Mol. Cell* **27,** 976–991
41. Ligon, L. A., Shelly, S. S., Tokito, M. K., and Holzbaur, E. L. (2006) Microtubule binding proteins CLIP-170, EB1, and p150Glued form distinct plus-end complexes. *FEBS Lett.* **580,** 1327–1332
42. Jiang, K., Toedt, G., Montenegro Gouveia, S., Davey, N. E., Hua, S., van der Vaart, B., Grigoriev, I., Larsen, J., Pedersen, L. B., Bezstarosti, K., Lince-Faria, M., Demmers, J., Steinmetz, M. O., Gibson, T. J., and Akhmanova, A. (2012) A Proteome-wide screen for mammalian SXIP motif-containing microtubule plus-end tracking proteins. *Curr. Biol.* **22,** 1800–1807
43. Dikovskaya, D., Schiffmann, D., Newton, I. P., Oakley, A., Kroboth, K., Sansom, O., Jamieson, T. J., Meniel, V., Clarke, A., and Näthke, I. S. (2007) Loss of APC induces polyploidy as a result of a combination of defects in mitosis and apoptosis. *J. Cell Biol.* **176,** 183–195
44. Aoki, K., and Taketo, M. M. (2007) Adenomatous polyposis coli (APC): a multi-functional tumor suppressor gene. *J. Cell Sci.* **120,** 3327–3335
45. Caldwell, C. M., and Kaplan, K. B. (2009) The role of APC in mitosis and in chromosome instability. *Adv. Exp. Med. Biol.* **656,** 51–64
46. Schindelin, J., Arganda-Carreras, I., Frise, E., Kaynig, V., Longair, M., Pietzsch, T., Preibisch, S., Rueden, C., Saalfeld, S., Schmid, B., Tinevez, J.-Y., White, D. J., Hartenstein, V., Eliceiri, K., Tomancak, P., and Cardona, A. (2012) Fiji: an open-source platform for biological-image analysis. *Nat. Methods* **9,** 676–682